Using RADARSAT constellation mission imagery to support talik mapping, Rankin Inlet, Nunavut, Canada

Wendy E. Sladen[1], Anne-Marie LeBlanc[1], Jason Chartrand[1] & Joost van der Sanden[2]

[1]*Geological Survey of Canada, Natural Resources Canada, Ottawa, Ontario, Canada*

[2]*Canada Centre for Mapping and Earth Observation, Natural Resources Canada, Ottawa, Ontario, Canada*

ABSTRACT

In continuous permafrost regions, taliks (perennially unfrozen ground) are mainly found beneath lakes that do not freeze to their bottom. Open taliks penetrate permafrost and provide conduits between surface water and groundwater. Knowledge of these pathways is critical for mining projects to understand mine-water inflow and assess the effects of mining activities on the groundwater-surface water system. Among other factors, talik extent is a function of lake bottom temperature, lake size, and the presence of shallow terraces, where bottom-fast ice (BFI) may occur. In this paper, we use RADARSAT Constellation Mission (RCM) imagery to support the classification of lakes with potential for open taliks in the Rankin Inlet area, Nunavut. We use RCM images collected in December 2022 and March 2023 to classify pixel values as BFI or floating ice (FI) based on image differencing and a threshold of -2 dB. The classified BFI showed good agreement with available bathymetry and field measurements. Ninety-nine percent (98.9%) of BFI mapped coincided with lake depths < 2 m. Lake depths < 0.5 m were classified as having on average 28.4% BFI. The lower proportion of BFI at the shallow depths is likely related to the timing of the reference RCM image. Classified BFI was less than half as extensive as lake terraces determined from multi-spectral imagery, suggesting that this methodology would result in a greater number of lakes with potential taliks. These results could be improved by obtaining imagery earlier in the season before BFI is established.

1 INTRODUCTION

In continuous permafrost regions, taliks, also known as perennially unfrozen ground, are expected beneath lakes deeper than the maximum ice thickness and for which annual mean lake-bottom temperature is typically above 0 °C. Conversely, permafrost is usually sustained below shallow lakes and lake terraces where water freezes to the bottom (Mackay 1992, Burn 2002). The timing and duration of lake-bed ice contact (bottom-fast ice; BFI), in addition to on-ice snow cover, affect lake-bottom temperature and dictate permafrost presence or absence (Stevens et al. 2010). Taliks may penetrate permafrost (open talik) beneath large lakes or be enclosed in permafrost (closed talik) beneath smaller lakes (Sumgin 1927). Knowledge of open taliks is critical for mining projects to understand mine-water inflow and assess the effects of mining activities on the groundwater-surface water system. However, open taliks are rarely observed directly (O'Neill et al. 2020), and assessments of sublacustrine open taliks have been achieved using numerical models (e.g., Ling et al. 2012; Golder 2021), airborne geophysics (Minsley et al. 2012), and geothermal modelling (e.g., Burn 2002). In a mineral resource-rich region, it is advantageous to develop a methodology based on remote sensing to locate where open taliks may be present. LeBlanc et al. (2022) used a supervised classification of multi-spectral imagery to map shallow lakes and lake terraces (< 2 m; first order estimate of permafrost presence) and deep waters (> 2 m; permafrost absence) at the regional scale. This mapping was then combined with a steady-state thermal model for open talik assessment (e.g., Burn 2002). However, this mapping approach relies on colour, which is influenced by the lake limnology and is not necessarily representative of depth (Duguay and Lafleur 2003) and, in addition, does not indicate BFI presence and duration. Space-borne synthetic aperture radar (SAR) has been an established tool for evaluating floating ice (FI) and BFI at high latitudes since the 1990s (Murfitt and Duguay 2021) and could, therefore, be used as proxy data for classification of lakes with potential open taliks. Active microwaves readily penetrate cloud, darkness, dry snow, and freshwater ice into the underlying water or sediment. High backscatter values have been observed in Ku-, X-, C-, and L-band SAR for FI due to the high dielectric contrast between ice and water and surface scattering at the rough ice-water interface, whereas the low dielectric contrast between ice and sediment causes the incident waves to be absorbed into the ground producing low backscatter values for BFI (Murfitt and Duguay 2021). As a result, the backscatter from BFI is usually significantly less than from FI. Sellman et al. (1975) and Mellor (1982) were among the first to show that BFI and FI can be differentiated from each other using X-band (9.6 GHz) and L-band (1.25 GHz) side-looking airborne radar whereas Jeffries et al. (1994) was one of the earliest studies to examine C-band (5.3 GHz) SAR images from ERS-1 data. Airborne and satellite SAR imagery have been applied to shallow lakes to get knowledge on lake ice regime and thickness, lake depth, and indirectly to assess permafrost and thermokarst processes, methane gas emissions, overwintering fish habitat, and freshwater availability for regions in Alaska, northern Manitoba, Mackenzie Delta, and Russia, and at the circumpolar scale (Murfitt and Duguay 2021). Threshold-based methods using C-band co-polarized signals (HH and VV) are the

https://doi.org/10.52381/ICOP2024.86.1

most common approaches used to classify FI and BFI (van der Sanden et al. 2012; Engram et al. 2018; Murfitt and Duguay 2021; Shaposhnikova et al. 2023). These methods use the difference in backscatter between FI and BFI to identify threshold(s) capable of differentiating between the two types of ice cover. Approaches vary from applying a single threshold for binary classification to a variable threshold determined through interactive threshold algorithms according to the diversity of the SAR datasets involved (e.g., French et al. 2004; Engram et al. 2018). Using this difference in backscatter, van der Sanden et al. (2012) classified BFI and FI by taking the difference of two images that straddle the winter season and classed BFI based on the reduction in backscatter.

In this paper, we use HH-polarized C-band RADARSAT Constellation Mission (RCM) imagery as a first exploration of this dataset. Working with only one freezing season and SAR platform, we use a simple image differencing method to support the classification of lakes with potential for open taliks for the Rankin Inlet area, Nunavut (LeBlanc et al. 2022). Our goal is to determine the lake ice regime (FI and BFI) for lakes in our study area. We assume that permafrost is sustained below lake areas with BFI, in other words that annual lake-bottom temperature is below 0 °C. We compare our results with available bathymetry (Golder 2012a, b), lake ice thickness measurements, and shallow water (< 2 m) extent determined from multi-spectral imagery analysis for the same area (LeBlanc et al. 2022).

2 Study Area

The 1242 km^2 study area is located near the Hamlet of Rankin Inlet, Nunavut (62°48′35″N, 92°05′58″W) and encompasses the Meliadine Mine (Figure 1). The topography is relatively flat with elevation ranging from sea level to 300 m; the Mine is about 60 m above sea level in low-lying topography with numerous lakes. The area was covered by the Laurentide Ice Sheet during the Wisconsinan glaciation until approximately 6 ka (Dyke 2004).

The region is situated within the continuous permafrost zone (Heginbottom et al. 1995) and permafrost thickness is estimated between 285 m and 430 m, with the thinner permafrost being near lakes, while the depth of the basal cryopeg is estimated to be between 280 m and 290 m below ground surface (Golder 2021). Modelled segregated ice abundance ranges from low to medium, the latter concentrated across the centre of the study area, near the Meliadine Mine, where fine-grained tills overlie sedimentary rocks (O'Neill et al. 2024). Kettle lakes and lakes shaped by glaciofluvial or glacial processes are common in the area (Golder 2014), in contrast to thermokarst lakes. The glacial and glaciofluvial deposits are oriented in a northwest-southeast direction, which is also the preferential lake orientation (Figure 1). Lakes cover 30% of the study area and range in size from 221 to 1.3 x 10^8 m^2 (Meliadine Lake) with an average and median lake size of 80,090 and 4,567 m², respectively. Maximum lake depth of about 100 surveyed lakes, around the Meliadine Mine, ranges from 0.11 to 23.5 m (Golder 2012a, b). The study area is in the Maguse River Upland ecodistrict of the Southern Arctic Ecoregion (Ecological Stratification Working Group 1995). Vegetation is primarily shrub and heath tundra dominated by ericaceous shrubs up to 50 cm in height and moss in well to moderately-drained areas and wet graminoid or sedge wetlands in poorly-drained areas (Campbell et al. 2012).

The mean annual air temperature (1981–2010) for Rankin Inlet is −10.5 °C (ECCC 2023). The average annual total precipitation is 311 mm, of which 41% falls as snow. The freezing season generally starts in early October. Ice covers start to form by the end of October and are completely formed in early November and remain until June (Golder 2014). Lake-ice thicknesses in the Meliadine Mine area, measured between 1998 and 2011, ranged from 1.0 to 2.3 m with an average thickness of 1.7 m (Golder 2014).

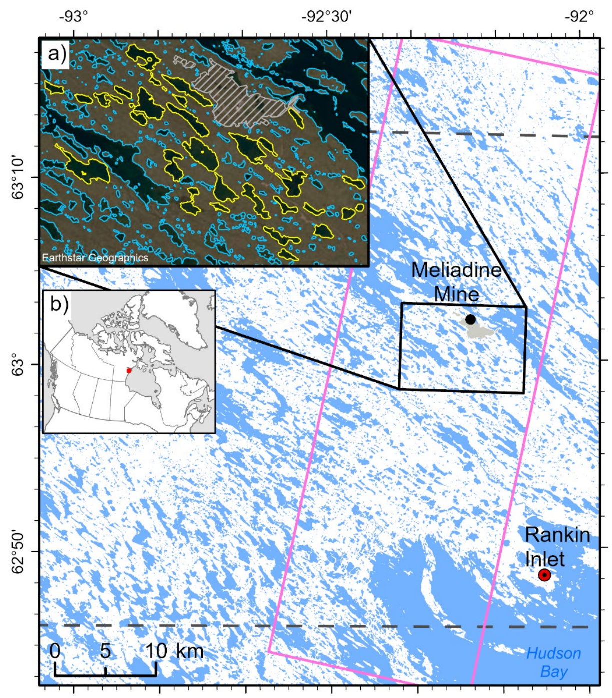

Figure 1. Map showing extent of RCM imagery (pink), bathymetry dataset (black) and north–south extent of shallow water mapping (dashed black). Rankin Inlet and Meliadine Mine are indicated. Inset a) shows lakes with bathymetry (yellow), Meliadine Mine is in grey hatching. Inset b) shows the study area location.

3 Methodology

3.1 Data

The SAR image dataset was obtained from the Canadian Space Agency's recently launched (2019) RADARSAT Constellation Mission. The RCM SAR images were collected from December 2022 to March 2023 in the Quad-Polarization (QP) mode, which has a spatial resolution of 9 m. The SAR data were accessed through the Canada Centre for Mapping and Earth Observation's Earth Observation Data Management System (EODMS). To determine the maximum extent of BFI, we selected an image pair that includes an early (reference) image acquired after freeze-up, but desirably before ice starts freezing to the bottom, and a later (working) image acquired at maximum ice thickness but prior to any surface snow melt (van der Sanden et al. 2012). We focused on the HH polarization as this is observed to have the greatest potential in detecting FI and BFI (van der Sanden et al. 2012). In addition, to eliminate the requirement to correct for incidence angle, images were selected from the same beam mode. Following these credentials QP13 images acquired on December 14, 2022 and March 16, 2023 were selected (Figure 2). The RCM SAR imaging parameters are found in Table 1.

Table 1. RCM SAR imaging details.

Parameter	Specification
Image Dates (yyyy-mm-dd)	2022-12-14, 2023-03-16
Operational Mode	Quad-Polarization
Beam Position	QP13
Spatial Resolution	9 m
Swath Width	20 km
Nominal NESZ*	-24 dB
Incidence Angle	31.24° (near), 32.85° (far)
Polarizations	HH, HV, VH, VV

*Noise Equivalent Sigma Zero

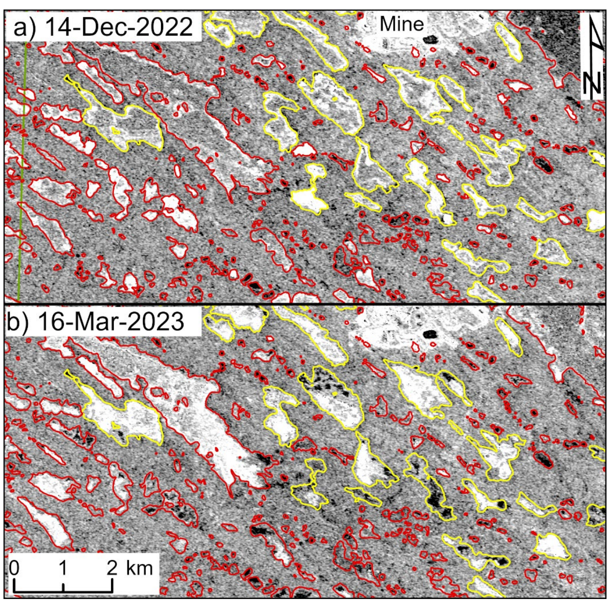

Figure 2. A close-up area of the RCM HH-polarization images in dB for a) 2022-12-14 (reference image) and b) 2023-03-16 (working image). Lakes with bathymetry are highlighted in yellow, all other lakes are outlined in red. Meliadine Mine is shown in upper right of images.

Daily mean air temperature determined from the meteorological data for Rankin Inlet (ECCC 2023), approximately 20–25 km SE of the study area, were used to determine the start and end of the 2022–2023 freezing season and select imagery dates. To evaluate the lake ice regime classification, we used the bathymetry dataset for 33 lakes near Meliadine Mine (Golder 2012a; LeBlanc et al. 2022). The bathymetric depth interval is 0.5 m (Figure 3). The CanVec 1:50,000 waterbody was used to restrict the analysis to lakes (NRCan 2017). The shallow lake and terrace (shallow waters) dataset produced from multi-spectral imagery (RapidEye) analysis and Maximum Likelihood Classification (LeBlanc et al. 2022) was used to compare the BFI extents.

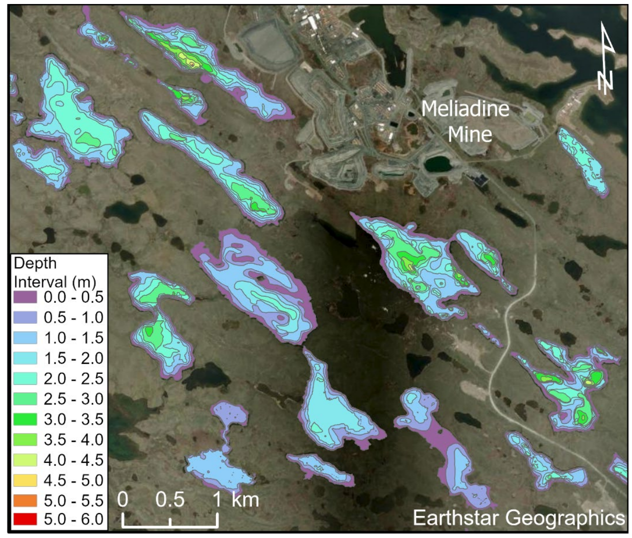

Figure 3. A subset of the lakes with bathymetry in the study area (modified from Golder 2012a, b). Depth intervals are in 0.5 m. The Meliadine Mine is visible near the top of the image.

3.2 Image Processing

Pre-processing of the SAR image data was conducted using the EODMS SAR Toolbox. The pre-processing of the Single Look Complexes included 1) radiometrically calibrating to Gamma Nought values; 2) converting complex values to detected values; 3) applying a GAMMA Map filter (Lopes et al. 1993) twice to reduce SAR speckle noise; and 4) orthorectification using rational function, nearest neighbour resampling, 5-m pixel spacing, Canada Digital Elevation Model, and projected to UTM/WGS84. The resulting TIF images were imported into PCI® Geomatica® Banff Focus and converted to a linear decibel (dB) scale using Raster Calculator and scaled for visual interpretation (Figure 2).

3.3 Lake Ice Regime Determination

Lake ice regime was determined using the image differencing method outlined in van der Sanden et al. (2012), where an earlier (reference) image is subtracted from a later (working) image. Image differencing was carried out using the Change Detection tool in PCI. The reference image (2022-12-14) is subtracted from the working image (2023-03-16) to determine the change in dB. To isolate the analysis to lakes only, the CanVec waterbody mask was applied. Based on observations in a similar Canadian Shield lake environment, a threshold of -2 dB, where values < -2 dB were classified as BFI and > -2 dB as

FI, was used for lake-ice classification (after van der Sanden et al. 2012). The raster results were imported into ArcGIS® Pro and cleaned using Majority Filter and Boundary Clean tools before converting to polygon shapefiles.

3.4 Analysis

The BFI and bathymetry datasets were overlain and the intersecting BFI area was calculated per lake depth interval in ArcGIS Pro. Percent BFI coverage per lake depth intervals was then determined in Excel®. This approach was also used to compare the BFI dataset with the shallow waters dataset determined from multi-spectral imagery.

4 RESULTS

4.1 Lake Ice Regime

There are 5387 lakes that lie completely within the 1242 km^2 study area, ranging in size from 221 m^2 to 9.5 x 10^6 m^2 (9.5 km^2). Lake size distribution is positively skewed; the median lake size is 4407 m^2, 75% of the lakes are smaller than 16,000 m^2, and 91% less than 64,000 m^2. Bottom-fast ice was detected in 2347 (43.6%) of the lakes by March 16, 2023 (Table 2). Of the lakes with BFI, the percent BFI areal coverage per lake ranged from 0.4% to 94.8% (average 25.5%, median 19.7%, standard deviation (SD) 21.2%). The 56.4% of lakes in which no BFI was detected, were generally a magnitude smaller in area than the lakes with BFI (Table 2). Isolated areas of BFI generally less than 1000 m^2 were mapped in the middle of less common larger, deeper lakes.

Table 2. Summary of lakes in the study area with and without bottom-fast ice (BFI) detected.

	Count	Area (m^2)			
		Mean	Median	Minimum	Maximum
All Lakes	5387	32,801	4407	221	9.5x10^6
Lakes with BFI	2347	71,268	18,759	368	9.5x10^6
Lakes with no BFI	3040	3104	1314	221	4.5x10^4

4.2 Bottom-fast Ice Validation

The lake ice regime results were compared against the set of bathymetric data and the 2023 field observations. Ice thickness was observed at 12 locations on five lakes in the southern portion of the study area in April 2023. Ice thickness ranged from 1.5 to 1.8 m (average 1.7 m, SD = 0.12) and was observed to be floating at all sites. The lake ice regime was classified as FI at the same locations.

Bottom-fast ice was detected in all lakes with bathymetric data (n = 33; Figure 4). Maximum lake depths ranged from 1.5 m (n = 33) to 6 m (n = 1), with 94% (n = 31) and 76% (n = 25) of the lakes reaching 2 m and 2.5 m depth, respectively. On average, 98.9% (SD = 2.1%) of the BFI determined per lake coincided with lake depths of ≤ 2.0 m and 90.8% (SD = 11.5%) corresponded to depths of ≤ 1.5 m. Less than 1% of BFI was mapped in areas deeper than 2 m and no BFI coincided with lake depths greater than 4.5 m.

Bottom-fast ice matched best with lake depth intervals 1–1.5 m and 0.5–1 m, with an areal coverage per lake averaging 67.6% (SD = 22.7%) and 59.4% (SD = 16.4%), respectively (Figure 4). At shallower (0–0.5 m) and deeper (1.5–2 m) depth intervals, the average areal extent of BFI per lake was less, averaging 28.4% (SD = 12.4) and 33.2% (SD = 34.5), respectively. Overall, BFI covered 49.3% (SD = 18.9%) of lake depths < 2 m on average.

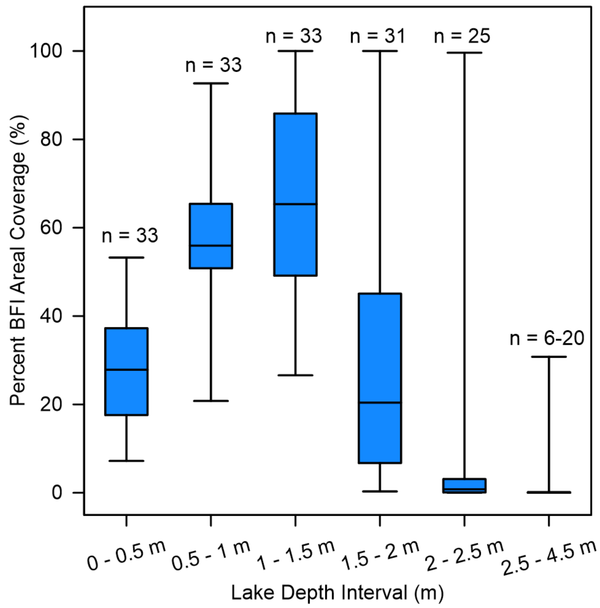

Figure 4. Box-whisker plot of the percent areal intersect of bottom-fast ice (BFI) and lake depth interval. n represents the number of lakes with the associated depth interval. The number of lakes to reach depths between 2.5 and 4.5 m ranges from 6 to 20.

4.3 BFI and Multi-spectral Classification of Shallow Waters

The BFI dataset was compared to the shallow waters dataset to evaluate the applicability of these two methods for estimating potential taliks in the Rankin Inlet area (Figure 5). Of the 3897 lakes within the overlapping BFI and shallow waters study areas, BFI was detected in 1846 (47%) of the lakes, slightly more than half of the lakes in which shallow waters were identified (3438, 88%). Bottom-fast ice was mapped in 1809 (52.6%) lakes with shallow waters and 37 lakes without shallow waters. On average, 72.8% of BFI coincided with the shallow water areas, whereas only 14.4% of shallow water areas were classed as BFI. Overall, for the lakes with BFI, the aerial extent per lake averages 25.6%, whereas shallow water extent averaged 65.1% in the lakes with shallow waters.

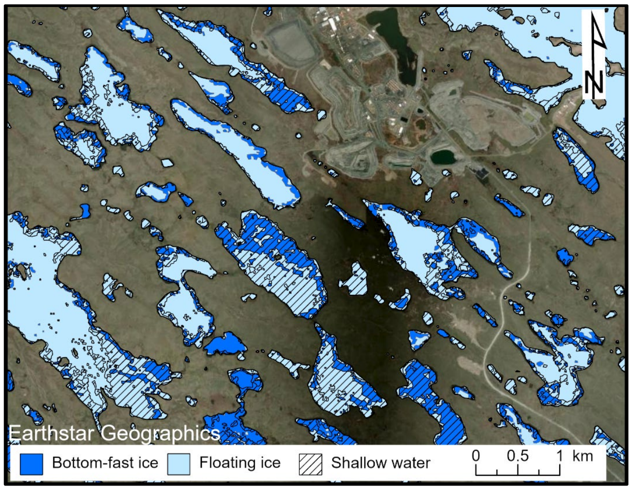

Figure 5. Example of lakes showing the extent of shallow waters (< 2 m) derived from RapidEye multi-spectral imagery (cross-hatched), bottom-fast ice (dark blue) and floating ice (light blue).

5 Discussion

Validation of the bottom-fast ice mapping results requires in situ field observations. Although no BFI was observed in the field during the study period, the limited ice-thickness measurements and available bathymetry were used to assess the BFI mapping results. Bottom-fast ice extent aligned well with the bathymetry with 90.8% and 98.9% of classified BFI corresponding to depths shallower than 1.5 m and 2 m, respectively. The 12 field ice-thickness observations were all of floating ice, matching 100% with the lake ice regime mapping at the same points. Lake depth intervals 0.5–1 m and 1–1.5 m, showed the highest BFI coverage, ranging from 59.4% to 67.6%. However, the correspondence between BFI extent and the shallowest lake depth interval (0–0.5 m) was lower than expected, averaging 28.4%, with an overall average of 49.3% for lake depths < 2 m.

To explain the lower values of BFI extent detected at shallower depths, ice growth was modelled using the weather station data at Ranking Inlet for 2022–2023 (ECCC 2023). Daily mean air temperatures first dropped below 0 °C on September 30 and remained below freezing as of October 21. Ice growth was estimated using the Stefan formula and freezing degree-days for windy lakes with no snow and lakes with snow (Michel 1971; Lunardini 1981; Figure 6). Model results indicate that ice cover started to form between October 8 and 16. Modelled ice thickness ranged from 0.5 m to 0.8 m on December 14 and from 1.0 to 1.6 m on March 16, the dates of the reference and working RCM images. The upper range of the modelled ice thickness is inline with field observations made in April 2023 suggesting that this model is appropriate for the area. This agrees with thicker ice expected in tundra environments where wind dominates control of ice formation leading to thinner and denser snowpack (Roy-Léveillée et al. 2014).

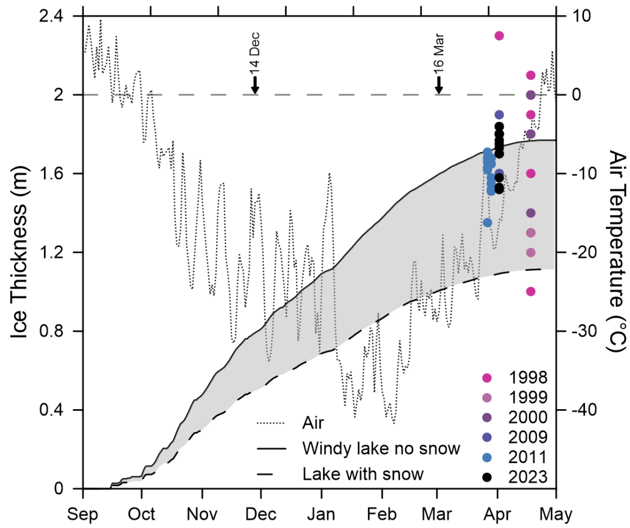

Figure 6. Daily mean air temperature for winter 2022 - 2023 for Ranking Inlet (dotted line; ECCC 2023), range of modelled ice thickness for lakes with (dashed line) and without snow (solid line) using freezing degree days (after Michel 1971). Ice thickness observations (dots) for 1998–2011 (Golder 2014) and 2023. The grey dashed line represents 0 °C air temperature and 2-m ice thickness. SAR image dates are noted.

With the March modelled ice thickness range of 1.0 to 1.6 m, we would expect the 1–1.5 m and 1.5–2 m lake depth intervals to be partially covered with BFI, which is the case. Likewise, we would expect the depth intervals 0–0.5 m and 0.5–1 m depths to be covered 100% with BFI, however, this is not observed. This is likely explained by the modelled ice thickness at the time of the reference image, where lake depths less than 0.5 to 0.8 m may already have bottom-fast ice. In this case, areas with BFI in the reference image would have low backscatter values and not produce a large negative change associated with BFI during image differencing and thus go unidentified (Figure 7). Likewise, this may be the case for the many small and thus presumably shallow lakes in the study area that had no BFI detected (Table 2). Indeed, of 78 lakes in the study area with known maximum depths (Golder 2012a, b), the 22 lakes for which no BFI was detected had a maximum depth on average of 0.65 m (SD = 0.3 m, range: 0.19–1.2 m). In addition, backscatter for some lakes has been observed to be consistently low for unknown reasons (van der Sanden et al. 2012).

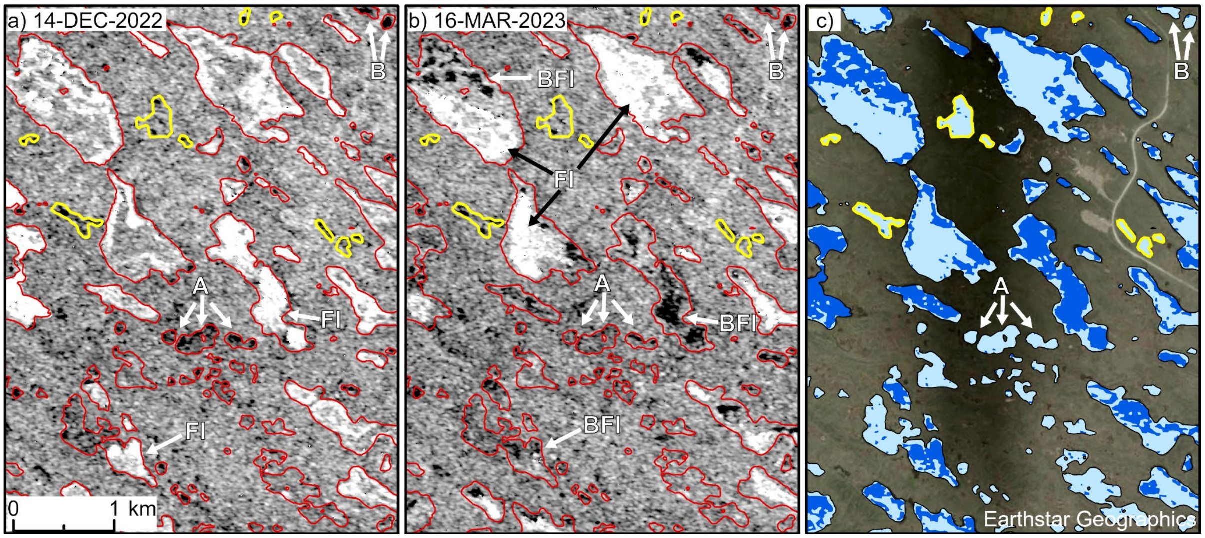

Figure 7. RCM HH images for a) 2022-12-14 and b) 2023-03-16, and c) resulting floating ice (FI, light blue) and bottom-fast ice (BFI, dark blue) classification for the same area. Lakes with a known maximum depth < 1 m are highlighted in yellow. "A" and "B" highlight lakes with low backscatter (dark) in both images resulting in ice classed as FI for these small lakes.

Acquisition of RCM imagery earlier in the season would help address the issue of missing early BFI in shallow lakes and lake terraces < 0.5 m deep. The modelled ice growth for 2022–2023, indicates that imagery acquired in early to mid-November when ice thickness is estimated to be less than 0.5 m, should improve BFI results. A study of lake-bottom temperature in the Rankin Inlet area confirms this timing of BFI in shallow waters (LeBlanc et al. 2024). In regions where there is a range of lake sizes, multiple early (reference) images may be required to detect BFI to account for the temporal window when smaller lakes are ice covered but ice is not bottom fast, and larger lakes are not yet frozen.

Other possible reasons for the lower correspondence between BFI and the shallower lake depths include change in lake levels. Lake levels in 2022 may have differed from those at the time the bathymetry was measured thus producing discrepancies in the areas classified to have BFI. In addition, the waterbody mask may not align perfectly with the current lakeshores and contribute to land being classified as FI or BFI. As for the isolated patches of BFI classed in the middle of deeper lakes, these have been observed in other studies (Duguay and Wang 2019; Shaposhnikova et al. 2023). Overestimation of BFI in these areas remains a challenge and is possibly due to ice cracking or local thinning (Pointner et al. 2019; Pointner and Barsch 2020).

Similarly to the bathymetry dataset, BFI extent matched well with the shallow waters extent (72.8%) but only 14.4% of shallow waters were mapped as BFI. The smaller number of lakes with BFI and smaller BFI extent relative to the multi-spectral classification of shallow waters may partly be explained by misinterpreting all light colors in the multi-spectral imagery as shallow areas less than 2 m. Field validation of water depth in 2023 indicated that some mapped terraces reached depths greater than 2 m. The overestimation of lake terrace extent may be related to lake limnology, one of the limitations of using multi-spectral imagery for lake depth (Duguay and Lafleur 2003). As a result, the shallow waters extent in the multi-spectral classification of lake bottom regimes may be overestimated. In addition, BFI extent may be underestimated in this study due to the timing of the reference image as previously mentioned. It is possible that agreement between the two datasets may improve if the full extent of BFI is captured. However, only the SAR classification provides information on BFI timing and duration, which remains an advantage for open talik assessment. These initial results indicate that the potential for taliks using BFI as a proxy for lake terrace width in steady-state thermal modelling governing open talik presence would result in a greater number of lakes with taliks and larger taliks with a greater potential for open taliks as compared to using the shallow waters dataset from multi-spectral imagery.

The BFI determined from the RCM SAR imagery processing shows good correspondence with the lake bathymetry and is a promising tool for use in talik mapping. Future work includes the collection and processing of multiple RCM scenes over the freezing season to determine the start of BFI establishment and growth. The timing and duration of BFI in conjunction with the monitoring of lake terrace temperature (LeBlanc et al. 2024) will be examined further to validate our talik mapping approach using BFI classification from SAR. In addition, our threshold value of -2 dB, based on past experience in a similar Canadian Shield lake environment, provided good results for this study area, however, further research will include the selection of threshold value(s) specific for the area.

6 Conclusions

Our results show that RCM SAR imagery can be successfully used to map bottom-fast ice using image differencing and is a promising tool for assessing lakes with potential open taliks in the Rankin Inlet area. Image differencing using RCM image pairs is a simple and time-efficient method for determining BFI. Timing of the early (reference) image is critical for determining the full extent of BFI and will vary depending on the lake morphology of the area under study. In lieu of in situ ice-thickness measurements and observations of ice regime, modelling ice growth with Stefan's formula can help in determining the timing of imagery required for BFI analysis. These results suggest that mapping BFI using this methodology provides a more conservative (i.e., greater) estimate of lakes with potential open taliks compared to supervised classification of multi-spectral imagery. Bottom-fast ice is likely underestimated in this study due to the timing of the first image being after BFI was established in shallow lake areas (less than 0.5–0.8 m). To improve BFI results for this study area, future work is underway to acquire imagery during the start of freeze-up with the intent to capture and map the full extent of BFI and refine the threshold. Exploration of the different polarizations, as well as combining beam modes to determine BFI timing and growth are also planned.

7 Acknowledgements

This work was supported by Natural Resources Canada's GEM-Geonorth program (contribution number 20230334). The author's wish to thank Naomi Short, CCMEO, for putting together the RCM imagery acquisition order and providing guidance on RCM imagery access. Field validation of ice thicknesses and water depths was made possible thanks to the support of Kangiqliniq HTO (Andre Aokaut) and the assistance provided by our wildlife monitor Roger Pilakapsi. The authors thank the reviewers for their comments which improved this manuscript.

10 References

Burn, C.R. 2002. 'Tundra lakes and permafrost, Richards Island, western Arctic coast, Canada', *Canadian Journal of Earth Science* 39(8), pp. 1281–1298. doi:10.1139/e02-035.

Campbell, M.W., Shaw, J.G., and Blyth, C.A. 2012. 'Kivalliq Ecological Land Classification Map Atlas: A Wildlife Perspective', *Government of Nunavut, Department of Environment* Technical Report Series #1-2012, 274 p. Available at: https://www.gov.nu.ca/environment/information/kivalliq-ecological-land-classification-map-atlas (Accessed: 15-sep-2023).

Duguay, C.R. and Lafleur, P. 2003. 'Determining depth and ice thickness of shallow sub-Arctic lakes using space-borne optical and SAR data', *International Journal of Remote Sensing* 24, pp. 475–489. Doi:10.1080/01431160304992.

Dyke, A.S. 2004. 'An outline of North American deglaciation with emphasis on central and northern Canada', *Developments in Quaternary Sciences* 2, pp. 373–424. Doi.org/10.1016/S1571-0866(04)80209-4.

ECCC 2023. *Environment and Climate Change Canada Canadian Climate Normals*. Available at: https://climate.weather.gc.ca/climate_normals/ (Accessed: 15-Sep-2023).

Ecological Stratification Working Group 1995. *A National Ecological Framework for Canada*. Agriculture and Agri-Food Canada, Research Branch, Centre for Land and Biological Resources Research and Environment Canada. State of the Environment Directorate, Ecozone Analysis Branch, Ottawa/Hull. Report and national map at 1: 7,500,500 scale. Available at: https://sis.agr.gc.ca/cansis/publications/maps/eco/all/districts/eco_all_districts_3m_nwtnu.jpg (Accessed: 15-sep-2023).

Engram, M., Arp, C.D., Jones, B.M., Ajadi, O.A., and Meyer, F.J. 2018. 'Analyzing floating and bedfast lake ice regimes across Arctic Alaska using 25 years of space-borne SAR imagery', *Remote Sensing of Environment* 209, pp. 660–676. doi:10.1016/j.rse.2018.02.022.

French, N., Savage, S., Shuchman, R., Edson, R., Payne, J., and Josberger, E. 2004. 'Remote Sensing of Frozen Lakes on the North Slope of Alaska', in *IEEE International Geoscience and Remote Sensing Symposium*. Anchorage, Alaska, United States: September 20–24, 2004, pp. 3008–3011. doi:10.1109/IGARSS.2004.1370330.

Golder 2012a. 'SD 7-1 Aquatics Baseline Synthesis Report, 1994 to 2009 - Meliadine Gold Project, Nunavut – Meliadine Gold Project', *Agnico-Eagle Mines Limited*, unpublished report prepared by Golder Associates Ltd., Doc 327-1013730076 Ver. 0. (report accessible at www.nirb.ca).

Golder 2012b. 'SD 7-2 2011 Aquatic Baseline Studies - Meliadine Gold Project, Nunavut – Meliadine Gold Project', *AgnicoEagle Mines Limited*, unpublished report prepared by Golder Associates Ltd., Doc 246-1013730076 Ver. 0. 77. (report accessible at www.nirb.ca).

Golder 2014. 'SD 6-1 permafrost thermal regime baseline studies – Meliadine Gold Project', *Agnico-Eagle Mines Limited*, unpublished report prepared by Golder Associates Ltd., Doc 225-1314280007 Ver. 0. (report accessible at www.nirb.ca).

Golder 2021. 'Meliadine Extension–2020 Thermal Assessment–Meliadine Gold Project', *Agnico-Eagle Mines Limited*, unpublished report prepared by Golder Associates Ltd., Doc 20136436-815-R-Rev2-2200. (report accessible at www.nirb.ca).

Heginbottom, J.A., Dubreuil, M.A., and Harker, P.A. 1995. 'Canada-permafrost', in *National Atlas of Canada, 5th edition.* Natural Resources Canada, MCR4177. doi:10.4095/294672.

Jeffries, M.O., Morris, K., Weeks, W.F., and Wakabayashi, H. 1994. 'Structural and stratigraphic features and ERS-1 synthetic aperture radar backscatter characteristics of ice growing on shallow lakes in NW Alaska, winter 1991-1992', *Journal of Geophysical Research: Oceans* 99(22), pp. 22459–22471. doi:10.1029/94JC01479.

LeBlanc, A.-M., Chartrand, J., and Smith, S.L. 2022. 'Regional assessment of the presence of taliks below Arctic lakes, Nunavut', *Geological Survey of Canada* Scientific Presentation 138, 1 poster. doi:10.4095/330205.

LeBlanc, A.-M., Sladen, W.E., and Faucher, B. 2024. 'Lake-bottom temperature on shallow and deep terraces for sublacustrine open talik assessment near Rankin Inlet, Nunavut, Canada', in *ICOP2024, 12th International Conference on Permafrost*. Whitehorse, Yukon, Canada: June 16–20, 2024.

Ling, F., Wu, Q., Zhang, T., and Niu, F. 2012. 'Modelling Open-Talik Formation and Permafrost Lateral Thaw under a Thermokarst Lake, Beiluhe Basin, Qinghai-Tibet Plateau', *Permafrost and Periglacial Processes* 23, pp. 312–321. doi: 10.1002/ppp.1754.

Lopes, A., Nezry, E., Touzi, R., and Laur, H. 1993. 'Structure detection and statistical adaptive speckle filtering in SAR images', *International Journal of Remote Sensing* 14(9), pp. 1735–1758. doi:10.1080/01431169308953999.

Lunardini, V.J. 1981. *Heat Transfer in Cold Climates*. New York, New York, United States: Van Nostrand Reinhold Company, 731 p.

O'Neill, H.B., Wolfe, S.A., and Duchesne, C. 2024. Modelled ground ice conditions in the Kivalliq region, Nunavut, Canada, in ICOP2024. Whitehorse, Yukon, Canada: June 16–20.

O'Neill, H.B., Roy-Leveillee, P., Lebedeva, L., and Ling, F. 2020. 'Recent advances (2010–2019) in the study of taliks', *Permafrost and Periglacial Processes* 31. pp. 346–357. doi:10.1002/ppp.2050.

Pointner, G. and Bartsch, A. 2020. 'Interannual variability of lake ice backscatter anomalies on Lake Neyto, Yamal, Russia', *GI Forum Journal* 8, pp 47–62. doi:10.1553/giscience2020_01_s47.

Pointner, G., Bartsch, A., Forbes, B. C., and Kumpula, T. 2019. 'The role of lake size and local phenomena for monitoring ground-fast lake ice', *International Journal of Remote Sensing* 40, pp. 832–858. doi:10.1080/01431161.2018.1519281.

Mackay, J.R. 1992. 'Lake stability in an ice-rich permafrost environment: Examples from the western Arctic coast, in R. Robarts and M. Bothwell (eds.), *Aquatic Ecosystems in Semi-arid Regions: Implications for Resource Management*. Saskatoon, Saskatchewan, Canada: August 27–30, 1990, pp. 1–25.

Mellor, J.C. 1982. *Bathymetry of Alaskan Arctic Lakes: A key to resource inventory with remote sensing methods*. PhD Thesis, Faculty of the University of Alaska. 361 p.

Michel, B., 1971. 'Winter Regime of Rivers and Lakes', *U.S. Army Cold Regions Research and Engineering Laboratory* Monograph III-B1a, 131 p.

Minsley, B.J., Abraham, J.D., Smith, B.D., Cannia, J.C., Voss, C.I., Jorgenson, M.T., Walvoord, M.A., Wylie, B.K., Anderson, L., Ball, L.B., Deszcz-Pan, M., Wellman, T.P., and Ager, T.A. 2012. 'Airborne electromagnetic imaging of discontinuous permafrost', *Geophysical Research Letters* 39(2), pp. 1–8. doi:10.1029/2011GL050079.

Murfitt, J. and Duguay, C.R. 2021. '50 years of lake ice research from active microwave remote sensing: Progress and prospects', *Remote Sensing of Environment* 264. doi:0.1016/j.rse.2021.112616.

NRCan 2017. 'Lakes, Rivers and Glaciers in Canada, CanVec Series, Hydrographic Features', 1:50,000, *Natural Resources Canada*. Available at: www.open.canada.ca.

Roy-Léveillée, P., Burn, C.R., and McDonald, I.D. 2014. 'Vegetation-permafrost relations within the forest-tundra ecotone near Old Crow, Northern Yukon, Canada', *Permafrost and Periglacial Processes* 25, pp. 127–135. doi:10.1002/ppp.1805.

Sellman, P.V., Weeks., W.F., and Campbell, W.J. 1975. 'Use of sidelooking airborne radar to determine lake depth on the Alaskan North Slope', *U.S. Army Cold Regions Research and Engineering Laboratory* Special Report 230.

Shaposhnikova, M., Duguay, C., and Roy-Léveillée., P. 2023. 'Bedfast and floating-ice dynamics of thermokarst lakes using a temporal deep-learning mapping approach: case study of the Old Crow Flats, Yukon, Canada', *The Cryosphere* 17(4), pp. 1697–1721. doi:10.5194/tc-17-1697-2023.

Stevens, C.W., Moorman, B.J., and Solomon, S.M. 2010. 'Modeling ground thermal conditions and the limit of permafrost within the nearshore zone of the Mackenzie Delta, Canada', *Journal of Geophysical Research* 115. doi:10.1029/2010JF001786.

Sumgin, M.I. 1927. *Permafrost Soil within the USSR*. 1st edition. Vladivostok, Russia: Far-Eastern Geophysical Observatory, 372 p.

van der Sanden, J.J, Geldsetzer, T., Short, N., and Brisco, B. 2012. *Advanced SAR Applications for Canada's Cryosphere (Freshwater Ice, and Permafrost)*, final technical report. Canadian Space Agency, Government Related Initiatives Program (GRIP), Natural Resources Canada, 54 pages. doi:10.4095/291867